RESEARCH PAPER

PCCP
www.rsc.org/pccp

Photodissociation dynamics of $SOCl_2$†

Alexei Chichinin,[ab] Tina S. Einfeld,‡[a] Karl-Heinz Gericke,[a] Jörg Grunenberg,[c] Christof Maul*[a] and Lars V. Schäfer§[c]

[a] *Institut für Physikalische und Theoretische Chemie, TU Braunschweig, Hans-Sommer-Straße 10, 38106 Braunschweig, Germany. E-mail: c.maul@tu-braunschweig.de*
[b] *Institute of Chemical Kinetics and Combustion, Novosibirsk, 630090, Russia*
[c] *Institut für Organische Chemie, TU Braunschweig, Hagenring 30, 38100 Braunschweig, Germany*

Received 23rd August 2004, Accepted 10th November 2004
First published as an Advance Article on the web 25th November 2004

New theoretical and experimental results for the ultraviolet photodissociation dynamics of thionyl chloride ($SOCl_2$) are presented and combined with existing data from a variety of sources in order to provide a unified view of the photodissociation dynamics of $SOCl_2$. Time-dependent density functional theory on the basis of the hybrid-type B3LYP functional was employed to calculate vertical excitation energies for the $SOCl_2$ parent molecule up to 6.3 eV. Three-dimensional (3D) imaging of photofragments was performed for a dissociation wavelength of 235 nm. Atomic chlorine fragments were observed in the $^2P_{3/2}$ ground state [Cl] and the $^2P_{1/2}$ excited spin–orbit state [Cl*] by employing resonance enhanced multi-photon ionization (REMPI) and time-of-flight (TOF) techniques. State-specific speed distributions and the speed dependence of the β anisotropy parameter were obtained from the full 3D momentum vector distribution by appropriate projection methods. Bimodal speed distributions for both spin–orbit states are evidence of a competition between the radical ($SOCl_2 \rightarrow SOCl + Cl/Cl^*$) and the three-body decay channel ($SOCl_2 \rightarrow SO + 2\,Cl/Cl^*$). No evidence of the molecular fragmentation channel ($SOCl_2 \rightarrow SO + Cl_2$) was found. With increasing fragment speed the β anisotropy parameter increases from 0.1 to 0.85 and 0.68 for Cl and Cl*, respectively, suggesting fragmentation *via* an excited A′ state for slow fragments and *via* an A″ state for fast fragments. The calculations allow for the first time to interpret all previous and new experimental data for the ultraviolet photodissociation of $SOCl_2$ by assuming simultaneous excitation of several excited electronic states giving rise to competing dissociation channels.

A. Introduction

The implementation of the 3D imaging technique that allows to monitor the full 3D momentum vectors of individual products of a chemical elementary reaction[1,2] has triggered the re-examination of the ultraviolet photodissociation of a series of tetratomic molecules which can, in principle, decay into three fragments. Especially the determination of the interdependence of the fragment speed distribution and the anisotropic spatial fragment distribution proved to be useful in the analysis of competing two- and three-body channels in the photodissociation of $CSCl_2$[3,4] and $COCl_2$.[5–7] In continuation of our previous studies on the photodissociation of structurally similar molecules we present here experimental and theoretical results of a photofragmentation study of the thionyl chloride molecule.

$SOCl_2$ has 58 electrons, 26 of which are valence electrons. It is a molecule of pyramidal geometry with a central sulfur atom at the top. It belongs to the C_s symmetry group with the symmetry plane containing the S=O double bond, and the electronic ground state is $X\ ^1A'$. Whereas until today only one early theoretical study exists on the electronic structure of $SOCl_2$ ground and excited electronic states,[8] experimentally the UV photolysis of the $SOCl_2$ molecule has been subject of several investigations.[9–14] The smooth absorption spectrum starts around 300 nm with distinct shoulders at 244 and 194 nm, as shown in Fig. 1[15] and can be described by a superposition of three main bands centered at 253, 235 and 191 nm.[16] The absorption spectrum has tentatively been assigned to partially overlapping electronic excitations from non-bonding electrons at the S and the Cl atoms to both anti-bonding π^*_{SO} and σ^*_{SCl} orbitals.[9] However, considering that within MO theory altogether 14 out of 26 valence electrons would be non-bonding at the S or Cl atoms, it would be surprising if this simple one electron picture were sufficient to understand the $SOCl_2$ photodissociation dynamics in detail, and a large number of excited electronic states must be expected to participate in the excitation and fragmentation of $SOCl_2$ even for only a narrow range of excitation energies. Therefore, we calculated vertical excitation energies, symmetries, and transition dipole moments for $SOCl_2$ using TDDFT. The theoretical results presented in this work explain our new experimental findings and previously existing experimental data equally well.

Previously, the photodissociation of $SOCl_2$ has been studied experimentally for photolysis wavelengths of 248, 235 and 193 nm. For all wavelengths, the following three dissociation channels are energetically accessible:

$$SOCl_2 + h\nu \rightarrow SO + Cl_2\ \lambda_{thr} = 557.1\ \text{nm} \quad (1)$$

$$\rightarrow SOCl + Cl/Cl^*\ \lambda_{thr} = 498.8\ \text{nm} \quad (2)$$

$$\rightarrow SO + 2Cl/Cl^*\ \lambda_{thr} = 263.5\ \text{nm} \quad (3)$$

They will be designated as the molecular, the radical, and the three-body decay channel, respectively.[17] Threshold

† Presented at the Third International Meeting on Photodynamics, Havana, Cuba, February 16–20, 2004.
‡ Present address: BASF AG, 67056 Ludwigshafen, Germany.
§ Present address: Max-Planck-Institut für biophysikalische Chemie, 37070 Göttingen, Germany.

DOI: 10.1039/b412797h

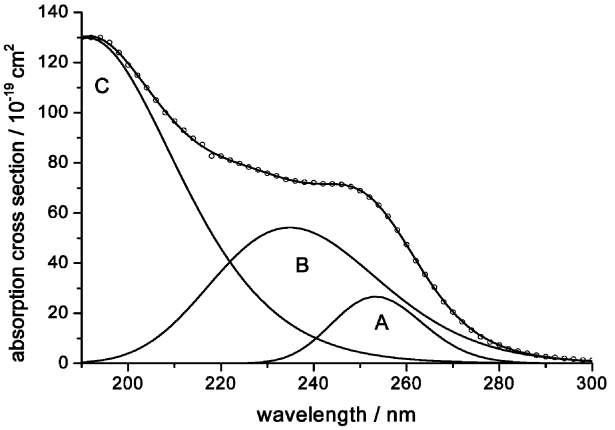

Fig. 1 Absorption spectrum of $SOCl_2$. Experimental data (open circles) are taken from Uthmann *et al.*[15] Three Gaussians A, B and C (solid lines) are fitted to the spectrum in order to elucidate the main contributions of excitations into different electronic states. The first major contribution at 253 nm can be assigned to excitation of the 2 ^{1}A′, 1 ^{1}A″ and 2 ^{1}A″ states. The second important contribution at 235 nm is associated with the excitation into the 3 ^{1}A′, 4 ^{1}A′ and 3 ^{1}A″ states. The third main contribution at 190 nm is mainly assigned to the 5 ^{1}A″ ← X ^{1}A′ transition.

wavelengths λ_{thr} are calculated for the generation of ground state fragments from thermodynamic data taken from refs. 18 and 19. From early photodissociation experiments it is known that at a dissociation wavelength of 248 nm the primary process is the fission of one sulfur–chlorine bond (channel 2).[9,10] Additionally, decomposition into three fragments (SO + 2Cl/Cl*) and a small contribution of the molecular channel (1) were observed.[9] At an excitation wavelength of 193 nm, the main dissociation channel is the three-body decay (3) accompanied by a small contribution of the radical channel (2).[9,10] Since then, UV photolysis has been used as a source of vibrationally and rotationally excited SO molecules in the X $^3\Sigma^-$, a $^1\Delta$ and b $^1\Sigma^+$ electronic states.[20–23] More recently, for all wavelengths detailed examinations of the $SOCl_2$ decay involving state-specific or spatially resolving detection of one or more photofragments have been performed from which it is clear that at least three different excited states must participate in the ultraviolet dissociation of $SOCl_2$.[14,16]

The scope of this article is to give a comprehensive description of the ultraviolet dissociation dynamics of the $SOCl_2$ molecule. To this end we first outline the results of TDDFT calculations (Section B). After a short description of our 3D imaging set-up (Section C), new experimental results obtained for the dissociation wavelength of 235 nm will be presented (Section D). Our new data and previously obtained experimental data for other dissociation wavelengths will be evaluated and analyzed in view of the results for the electronic structure of $SOCl_2$ obtained from our calculations (Section E). To the level of theory we employed, all experimental evidence obtained so far can be rationalized from a wavelength dependent simultaneous excitation of several of the 10 lowest electronically excited states of the $SOCl_2$ molecule producing chemically as well as physically different species *via* the molecular, the radical, and the three-body decay channels in competition.

B. Theoretical results

Time-dependent density functional theory[24] based on the hybrid functional B3LYP[25] has been applied for the investigation of electronically excited states of thionyl chloride $SOCl_2$. All quantum chemical calculations were carried out using the GAUSSIAN-98 program.[26] The 6-311G+(3df) triple zeta basis set was used for all calculations. As a first step, the geometry of $SOCl_2$ in the ground state has been studied. The calculated bond lengths and angles are in very good agreement with experimental observations as listed in Table 1 from electron diffraction[27–29] or microwave spectroscopy.[30,31]

Table 1 $SOCl_2$ ground state geometries. Comparison of molecular parameters obtained in our calculations with experimental data (refs. 27–31)

Parameter	This work	ref. 27	ref. 28	ref. 29	ref. 30	ref. 31
r(S–O)/pm	143.8	145	144.4	144.3	144	142.8
r(S–Cl)/pm	211.2	207	207.6	207.6	207.2	207.4
∠(Cl–S–O)/°	107.8	106	107.3	106.3	108.0	108.0
∠(Cl–S–Cl)/°	98.2	114	96.2	96.1	97.2	97.0

Vertical excitation energies have been calculated for the optimized ground state geometry given in Table 1. No Rydberg excitations are expected below 8 eV.[32] The lowest 10 excited singlet states covering the energy range up to 6.3 eV are listed in Table 2. The lowest singlet state 2 ^{1}A′ is of A′ symmetry, located at an excitation energy of 4.63 eV. It has a relatively large oscillator strength of 0.024 and is therefore likely to be identified as the main contributor to the absorption feature A in Fig. 1. The 2 ^{1}A′ state and two electronic states of A″ symmetry, the 1 ^{1}A″ state at 4.78 eV and the 2 ^{1}A″ state at 4.96 eV, can be accessed with a 248 nm (5.0 eV) photon. At slightly higher excitation energies there follows a group which consists of three states 3 ^{1}A′, 3 ^{1}A″ and 4 ^{1}A′ at 5.30, 5.37 and 5.46 eV, respectively. The prominent absorption feature B in Fig. 1 is likely to be due mainly to the strong transition to the 3 ^{1}A″ state with an oscillator strength of 0.057. This group is almost exactly located at the energy of a 235 nm (5.3 eV) photon. Within the accuracy of the calculations and due to the energy broadening discussed below all of these states are expected to be accessible at an excitation wavelength of 235 nm in addition to the lower states discussed above. Four more states can be accessed by absorption of 193 nm (6.4 eV) light: 5 ^{1}A′, 4 ^{1}A″, 6 ^{1}A′ and 5 ^{1}A″ at 5.66, 5.86, 6.07 and 6.26 eV, respectively. The latter with the high oscillator strength of 0.081 is most likely to be responsible for the absorption feature C in Fig. 1.

While the accuracy of TDDFT calculations is difficult to determine in general, for $SOCl_2$, where no Rydberg states are involved and where the first ionization potential of 11.12 eV[33] is significantly higher than the considered states, the accuracy for excited state energies reaches the accuracy of sophisticated quantum chemical methods. Comparing our calculated excitation energies for transitions with large oscillator strengths to the main absorption features of Fig. 1 results in deviations of the order of 0.2 eV.

Table 2 $SOCl_2$ electronically excited singlet states (ΔE: vertical excitation energy, f: oscillator strength, β_{Cl}: limiting Cl anisotropy parameter for instantaneous decay from the ground state equilibrium geometry)

Symmetry	ΔE/eV	f	β_{Cl}
2 ^{1}A′	4.63	0.024	(+0.28)
1 ^{1}A″	4.78	0.0001	+0.71
2 ^{1}A″	4.96	0.009	+0.71
3 ^{1}A′	5.30	0.002	+0.27
3 ^{1}A″	5.37	0.057	+0.71
4 ^{1}A′	5.46	0.004	+0.06
5 ^{1}A′	5.66	0.004	−0.66
4 ^{1}A″	5.86	0.004	+0.71
6 ^{1}A′	6.07	0.005	+0.23
5 ^{1}A″	6.26	0.081	+0.71

A crude estimate of the broadening of the calculated energies yields widths of 0.2–0.5 eV equivalent to excited state lifetimes between 60 and 150 fs which are typical for repulsive states. This estimate is based on the number of states spanning the wavelength range from 190 to 250 nm, considering the different oscillator strengths of Table 2. Thus, a photon induced transition to an excited state is likely to start for photons with energies of about 0.5 eV less than its vertical excitation energy, and states which are separated by less than 0.5 eV in their vertical excitation energies are likely to be simultaneously excited.

C. Experimental

We obtained the full 3D momentum distribution of Cl and Cl* photofragments from the photolysis of $SOCl_2$ at 235 nm. A more detailed description of the experimental set-up and the novel position sensitive detector (PSD) has been published elsewhere.[1,7] Briefly, it consists of a combination of a home-built single-field time-of-flight (TOF) mass spectrometer and a position sensitive detector.[34–36] The spectrometer was evacuated to a base pressure of about 10^{-8} mbar by a turbo molecular pump system. Thionyl chloride was constantly cooled to −20 °C (gas pressure: *ca.* 15 mbar at −20 °C) to prepare a mixture of 0.5% $SOCl_2$ in helium. Measurements of the room-temperature sample were performed at a pressure of 10^{-7} mbar, corresponding to a $SOCl_2$ density of 10^7 cm^{-3}. Measurements of jet-cooled samples at a temperature of 8 K agree with the results from the bulk measurements, but were not further analyzed due to background interference.

Simultaneous dissociation and state-selective detection of chlorine atoms were performed using one dye laser pumped by a Nd : YAG laser (Coherent, Infinity 40–100). The dye laser (Lamba Physik, Scanmate) was operated with Coumarin 47 at a repetition rate of 100 Hz, its light was frequency doubled by a BBO crystal and focused by a 20 cm lens in order to decrease the reaction volume to 5×10^{-4} mm^3. The energy of the frequency-doubled light amounted to 5–10 μJ per pulse. The energy was kept low to detect approximately one Cl^+ ion per ten laser pulses for avoiding saturation of the dissociation step and kinetic energy transfer to the fragments due to space charge effects. The laser beam and the detector axis were orthogonal in the interaction region. Although a single 3D image contains the complete information about the fragmentation process, the polarization of the laser could be changed by a half wave plate in order to detect and avoid experimental artifacts. Typically, the acceleration voltage was 800 V in the acceleration tube of the TOF spectrometer corresponding to an acceleration field of 16 kV m^{-1}.

The ^2P_J state of the chlorine atom is split by 882 cm^{-1} (0.11 eV) due to spin–orbit coupling into Cl($^2P_{3/2}$) and Cl*($^2P_{1/2}$). Both states were detected by a (2 + 1) REMPI process. The ground state was probed *via* the ($^2D_{3/2} \leftarrow {}^2P_{3/2}$) transition at 235.336 nm, the excited state by the ($^2S_{1/2} \leftarrow {}^2P_{1/2}$) transition at 235.205 nm.[37,38] Typically the dye laser was scanned over a range of ±0.003 nm around the chlorine atom transitions accounting for the Doppler broadening. Signals were processed by the electronic set-up, digitized by time-to-digital converters, accumulated over 2×10^5 laser shots and saved on-line by a personal computer. The analyzing procedure is described in detail elsewhere.[7]

The PSD includes a delay-line anode introduced into the spectrometer chamber right behind the double stage multi-channel plates. The PSD allows us to monitor all three components of the momentum vector from the measured position of the particle on the detector and its arrival time. Therefore, a full 3D velocity distribution is observed and the complete information about the speed distribution and the speed dependent β parameter is obtained.

D. Experimental results

(i) Spin–orbit branching ratio

The spin–orbit branching ratio was obtained by scanning the laser over the two resonance transitions of Cl and Cl*. The measurements were repeated at different laser light intensities. Integrating the area under the Doppler profiles results in a signal ratio S(Cl*)/S(Cl) of 0.5 ± 0.04. Taking the ratio of transition probabilities of 1.06 ± 0.17[39] into account we determined a Cl* yield ϕ(Cl*) = 0.35 ± 0.06 where ϕ is defined as the ratio of the number of excited state atoms P(Cl*) to the total number of chlorine atoms: ϕ(Cl*) = P(Cl*)/[P(Cl) + P(Cl*)]. This value is in perfect agreement with previously determined branching ratios[14,16] if the most recently observed transition probabilities for the chlorine spin–orbit states are taken into account.[39] Although the value of 0.35 coincides with the value of a statistical distribution (0.33), it does not mean that the decay proceeds statistically. On the contrary, the value of 0.35 is obtained from averaging over several highly non-statistical decay channels. This fact illustrates the necessity for monitoring the decay dynamics in the greatest possible detail.

(ii) Speed distributions

In our experiment the full 3D velocity distribution F of photofragments is monitored. The distribution F resulting from fragmentation following one-photon excitation of the parent molecule can be expressed in spherical coordinates v, θ and ϕ attached to the electric field vector $\boldsymbol{E}$:

$$\boldsymbol{F}(v,\theta,\varphi) = \frac{f(v)}{4\pi v^2}[1 + \beta(v)P_2(\cos\theta)] \qquad (4a)$$

Here, F is the 3D velocity vector distribution, v is the 1D absolute value of the speed and $f(v)$ its 1D distribution, β is a speed-dependent anisotropy parameter, P_2 is the second Legendre polynomial and θ is the polar angle of the velocity vector $\boldsymbol{v}$ with the electric field vector $\boldsymbol{E}$. The absence of the azimuthal angle ϕ in eqn. (4a) is a consequence of the cylindrical symmetry of F with respect to $\boldsymbol{E}$. The 3D distribution (4a) is normalized such that

$$\int\int\int v^2 \sin\theta \, dv \, d\theta \, d\varphi \, F(v, \theta, \phi) = 1 \qquad (4b)$$

and

$$\int f(v) dv = 1 \qquad (4c)$$

The anisotropy parameter β can take on values between −1 and +2. A parameter value of $\beta = 0$ describes an isotropic distribution (no θ dependence), whereas $\beta = -1$ describes a "perpendicular" distribution ($F \propto \sin^2\theta$) and $\beta = +2$ describes a "parallel" distribution ($F \propto \cos^2\theta$).[40,41]

The value of the β parameter for an immediate decay on one single excited potential energy surface depends only on the geometry of the molecule and the direction of the transition dipole moment which itself is determined by the symmetries of the initial and the final state in the excitation step. The β parameter is related to the angle ξ of the transition dipole moment μ with the fragment velocity vector $\boldsymbol{v}$ by[42]

$$\beta = 2P_2(\cos\xi) \qquad (5)$$

1D speed distributions $f(v)$ are obtained from the 3D momentum distributions by integrating over the angular coordinates θ and ϕ. The results are shown in Fig. 2. Although both distributions are bimodal, a remarkably different behavior of the two spin–orbit components with respect to their kinetic energy acquisition in the photodissociation is obvious. The distribution of ground state Cl is of double peak shape, with the peaks at 900 and 2500 m s^{-1} separated by a minimum at 1800 m s^{-1}. In the case of excited state Cl* the distribution is singly peaked at 2500 m s^{-1}, accompanied by a shoulder in the

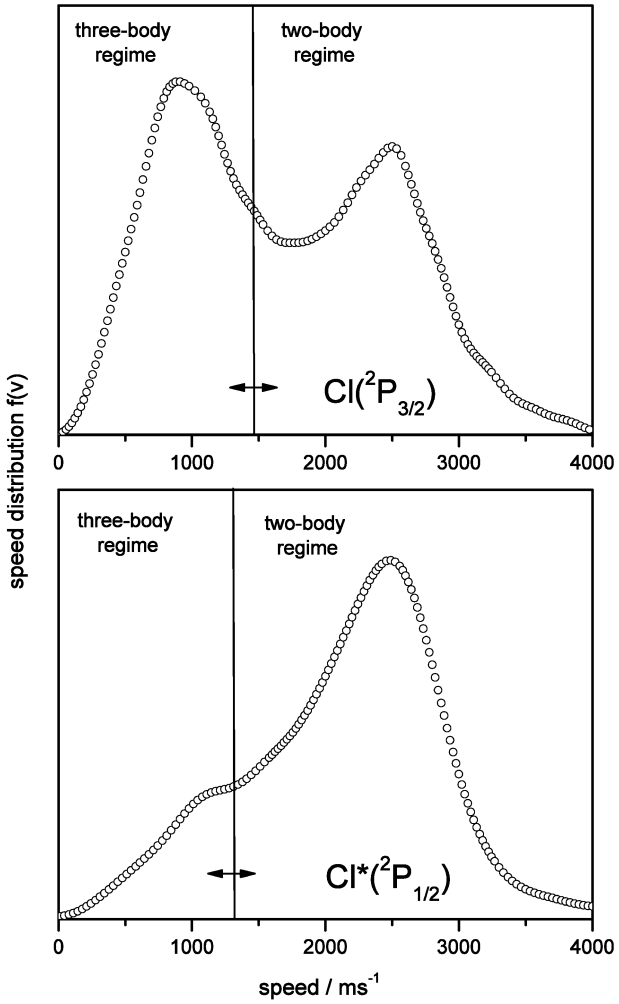

Fig. 2 State-specific speed distributions. The energetic boundary between the three-body channel (3) and the radical channel (2) is marked by the vertical line. The horizontal error bar results from thermal parent molecule motion.

low speed region around 1200 m s^{-1}. The small contributions above 3500 m s^{-1} belong to minor signals of ^{37}Cl, resulting from onsetting overlap of the ^{37}Cl image with the ^{35}Cl image. Such a spin–orbit state specific behavior is not uncommon and has been observed for a variety of molecules, including $COCl_2$,[5–7] $CSCl_2$ [3,4] and S_2Cl_2 [43] which have previously been studied in our laboratory.

The observed speed distributions as depicted in Fig. 2 are in very good agreement with previously published data.[14,16] Note that the data shown in Fig. 2 were obtained in a 300 K bulk experiment, hence the slow chlorine atoms cannot be ascribed to the dissociation of $SOCl_2$ within a cluster as was suggested previously.[12,14] Rather, the slow component of Cl and of Cl* must be generated in the UV dissociation of the isolated parent molecule and thus carry valuable information about its dissociation dynamics. Threshold speeds for the radical and the three-body decay channels (2) and (3) are 3290 and 1480 m s^{-1} (3225 and 1330 m s^{-1}) based on thermodynamic data from ref. 18 (bracketed values are for Cl*). The three-body decay threshold speed is accordingly marked in Fig. 2 together with a 250 m s^{-1} uncertainty from thermal parent molecule motion. It is tempting to associate the fast and the slow components with products of the radical channel (2) and the three-body decay channel (3), respectively, where the three-body decay mainly produces ground state Cl while the radical channel generates both Cl and Cl* spin–orbit states. However, for both spin–orbit states the slow component seems to reach across the boundary delimiting the three-body decay into the energetic regime associated with the radical channel (2). Whereas the distinction between three-body and radical decay is a strict one from purely energetic reasoning, it is not evident whether the two dissociation channels (2) and (3) can also be identified with initial excitation of the $SOCl_2$ molecule in different electronic states, as was previously suggested.[14,16] To this end the analysis of the speed dependence of the β parameter serves as a more valuable tool than the integrated speed distributions $f(v)$. The speed dependence $\beta(v)$ of the spatial fragment distribution will be discussed in the subsection below.

(iii) Speed dependence of the spatial fragment distribution

In experiments employing rotatable detectors the distribution F can be directly measured by placing the detector at the desired place defined by (θ,ϕ). In order to extract the speed dependence of the β parameter from the 3D momentum vector distribution, the 3D distribution $F(v,\theta,\phi)$ must be integrated over the azimuthal angle ϕ and the resulting signal distribution has to be evaluated with respect to the polar angle θ in dependence on the speed v. Note that this integration over ϕ does not remove the sin θ angular dependence of the volume element in eqn. (4b), so that it is useful to define

$$F_\theta(v,\theta)\mathrm{d}\theta\,\mathrm{d}v = \int \mathrm{d}\varphi v^2 \sin\theta\,\mathrm{d}\theta\,\mathrm{d}v F(v,\theta,\varphi) = \frac{f(v)}{2}(1+\beta(v)P_2(\cos\theta))\sin\theta\,\mathrm{d}\theta\,\mathrm{d}v \quad (6a)$$

which is normalized according to

$$\int \mathrm{d}v \int \mathrm{d}\theta\; F_\theta(v,\theta) = 1 \quad (6b)$$

in agreement with eqns. (4). F_θ now allows a direct comparison with the experimentally observed data.[2,7]

Fig. 3 shows the speed dependent β parameters for Cl and Cl* as obtained from this procedure. In the case of ground state Cl the β parameter belonging to particles with low speed is only slightly positive, which means that the slow ground state Cl fragments are almost isotropically distributed whereas in the region of high speed the β parameter increases to 0.85 ± 0.1. It is important to note that the strong β parameter increase is shifted from the observed speed distribution minimum at 1800 m s^{-1} and the energetic limit for the three-body decay at 1480 m s^{-1} by 300 and 620 m s^{-1}, respectively, towards higher recoil speeds. In the case of excited state Cl* the anisotropy behavior is very similar to the ground state Cl anisotropy. At 2100 m s^{-1} the value of the β parameter increases rapidly to a value of 0.68 ± 0.1. Analogously to ground state Cl, the increase of the β parameter is shifted with respect to the increase in intensity and the energetic limit for the three-body decay.

Since our experiment was performed for a room temperature sample, the significance of this shift in the β parameter increase must be carefully assessed. When observing a light fragment from a heavy parent molecule, rotation of the parent is the dominant source of β parameter reduction. If β' is the reduced and β the original anisotropy parameter, the reduction is given by[40,42]

$$\beta'(v) = \beta(v)P_2(\cos\alpha) \quad (7)$$

The angle α characterizes the deviation of the overall fragment recoil direction from the direction induced by the bond cleavage and is related to the thermal tangential velocity component v_t and the speed v acquired in the dissociation by:

$$\alpha = \arctan\frac{v_t}{v} \approx \frac{v_t}{v} \quad \text{for} \quad v_t \ll v. \quad (8)$$

Considering a pseudo-diatomic molecule composed of two masses m_1 and m_2, classically the maximum of the tangential

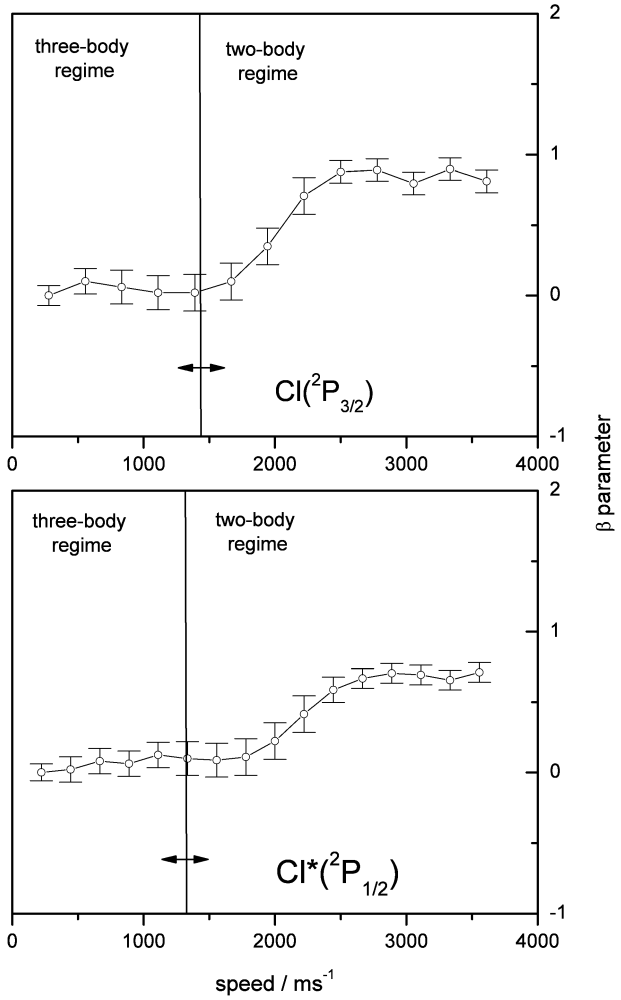

Fig. 3 State-specific speed dependence of the β anisotropy parameter. The energetic boundary between the three-body channel (3) and the radical channel (2) is marked by the vertical line. The β parameter increase at speeds higher than the boundary value is evidence that two- and three-body fragmentation cannot simply be associated with excitation into different excited states of the parent molecule. The horizontal error bar results from thermal parent molecule motion.

speed distribution function $f(v_t)$ lies at:

$$v_t^m = \sqrt{\frac{kT}{m}} \text{ where } m = m_1(m_1 + m_2)/m_2. \qquad (9)$$

For Cl fragments generated from $SOCl_2$ ($m_1 = m_{Cl}$, $m_2 = m_{SOCl}$) photodissociation recoiling at a speed of 1800 m s^{-1}, rotational motion of room temperature parent molecules will reduce the β parameter by 2.3%. The effect of translational motion will be even smaller because of the larger mass of the parent molecule and because translational motion takes place in three dimensions instead of only two considered for rotation. Thus, we conclude that the delayed β parameter shift must be caused by the dynamics of the photodissociation process and is not an experimental artifact.

E. Discussion

Table 3 lists the asymptotic product states which are energetically accessible by absorption of an ultraviolet photon with a wavelength $\lambda \geq 193$ nm together with their dissociation energies ΔE_p and threshold wavelengths λ_{thr}. Dissociation energies were calculated from 0 K enthalpies of formation, uncertainties are 0.01 eV.[18] The small excitation energies of the SO(a $^1\Delta$) state of 0.79 eV[19] and of the SO(b $^1\Sigma^+$) state of 1.30 eV[19] give rise to three accessible product states, each in the molecular channel (1) and the three-body channel (3). Additionally, in the molecular channel also electronically excited Cl_2(B $^3\Pi_{0+u}$) at 2.21 eV[19] above the ground state can be produced. Electronic excitation of the SOCl radical, although previously suggested,[12] has not been considered since *ab initio* calculations failed to confirm the proposed excited state around 1.1 eV.[44] In agreement with this result, our own calculations suggest electronically excited states for SOCl only above 3 eV. Fig. 4 shows an overview of the calculated vertical excitation energies for the 10 lowest singlet electronic states as listed in Table 2 in conjunction with the asymptotic product states listed in Table 3 and the excitation wavelengths used in our own and several previous photodissociation experiments.

Before our new experimental results will be analyzed in detail, in the following three sections the to-date existing experimental evidence will be interpreted in view of the results of our TDDFT calculations. The employed dissociation wavelengths will be individually addressed in the following paragraphs.

(i) Photolysis at 248 nm

Previous experimental data at a dissociation wavelength of 248 nm were obtained in conceptually different experiments. Huber and co-workers employed spatially resolving photofragment translational spectroscopy (PTS) measurements capable of monitoring the complete set of all fragment species without quantum state resolution, while Weiner and co-workers employed state-specific laser induced fluorescence detection of SO(X $^3\Sigma^-$) without spatial or kinetic energy resolution.

The PTS measurements are evidence that the $SOCl_2$ decay at a dissociation wavelength of 248 nm mainly proceeds along the radical channel (2) under significant excitation of the SOCl fragment from initial preparation of a state of A″ symmetry with a decay time of less than 1 ps.[12] A small contribution of less than 3% of the molecular channel (1) was also determined analyzing time-of-flight profiles of Cl_2 fragments where almost all SO partner fragments are electronically excited into the b $^1\Delta$ state.[12] For this channel, the Cl_2 spatial distribution suggests a decay *via* an initially excited state of A′ symmetry.[12] Some slow chlorine fragments were originally attributed to the formation

Table 3 Asymptotic product energy levels energetically accessible in the decay channels (1) to (3). (ΔE_p: dissociation energies with respect to $SOCl_2$(X ^{1}A′), λ_{thr}: threshold wavelength). Energy values are taken from refs. 18 and 19. Energy uncertainties are 0.01 eV.[18]

Decay channel	Products	ΔE_p/eV	λ_{thr}/nm	
Molecular	SO(X $^3\Sigma^-$) + Cl_2(X $^1\Sigma_g^+$)	2.23	557.1	spin-forbidden
Radical[a]	SOCl(X ^{2}A″) + Cl(^{2}P$_J$)	2.49	498.8	
Molecular	SO(a $^1\Delta$) + Cl_2(X $^1\Sigma_g^+$)	3.01	411.9	
Molecular	SO(b $^1\Sigma^+$) + Cl_2(X $^1\Sigma_g^+$)	3.53	351.3	
Molecular	SO(X $^3\Sigma^-$) + Cl_2(B $^3\Pi_{0+u}$)	4.43	275.5	
Three-body	SO(X $^3\Sigma^-$) + 2Cl(^{2}P$_J$)	4.71	263.5	
Three-body	SO(a $^1\Delta$) + 2Cl(^{2}P$_J$)	5.49	225.8	
Three-body	SO(b $^1\Sigma^+$) + 2Cl(^{2}P$_J$)	6.01	206.3	

[a] No electronic excitation of SOCl considered (see text for details).

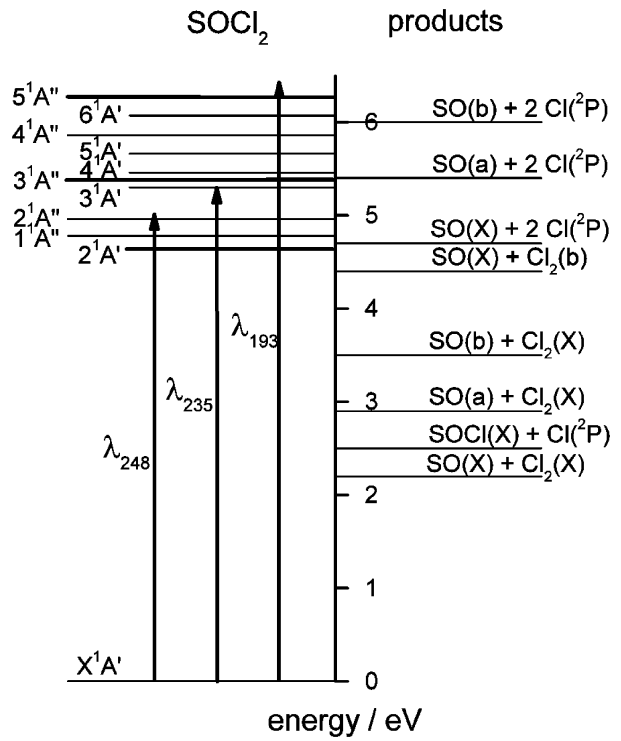

Fig. 4 Left panel: Calculated vertical excitation energies for the lowest 10 singlet states. Photon energies for excitation at 248, 235 and 193 nm are marked by solid arrows. Bold levels have high oscillator strength. Right panel: Asymptotic energy levels for products from molecular (1), radical (2), and three-body decay (3) channels in their energetically accessible electronic states.

of $SOCl_2$ clusters and a suggested internal energy dependence of SOCl fragmentation in the ionizer of the mass spectrometer. We would like to suggest, however, that the slow chlorine fragments are rather produced in the three-body decay process (3).

In agreement with the PTS experiment, in the LIF study[13] a lower limit of 0.13 ± 0.07 for the quantum yield of the SO producing channels (1) and (3) was determined. A small portion of *ca.* 6% of the observed SO($X\ ^3\Sigma^-$) fragments were vibrationally excited to such an extent that they necessarily had to be produced by the molecular channel (1) with a highly excited Cl_2 fragment as partner, consistent with an electronic excitation of the Cl_2 partner molecule into its $B\ ^3\Pi_{0+u}$ state. Since the LIF measurements[13] were not performed under collision-free conditions, no information about the kinetic energy content of the remaining SO($X\ ^3\Sigma^-$) fragments is available, so that a determination of the branching ratio between channels (1) and (3) was not possible. The PTS results suggest however, that SO($X\ ^3\Sigma^-$) must be produced in the three-body decay channel (3) since the Cl_2 observed in the PTS study[12] was assigned to electronically excited SO($b\ ^1\Sigma^+$) partner fragments which could not be observed in the LIF experiment[13] and since the total yield of Cl_2 found in the PTS study[12] is significantly smaller than the SO($X\ ^3\Sigma^-$) yield determined in the LIF study.[13] Then, the slow chlorine fragments observed in the PTS study[12] at mass 35 are the counterparts to the vibrationally cold ground state SO fragments which are all produced by the three-body decay channel (3).

In view of our calculations we suggest the following fragmentation scheme of $SOCl_2$ following excitation at 248 nm: The $2\ ^1A''$ state and the $2\ ^1A'$ state are simultaneously excited. The $1\ ^1A''$ state which, in principle, can also participate in the fragmentation has not been considered due to its extremely small oscillator strength. The $2\ ^1A''$ state is the main dissociation channel producing the majority of the fragments. Fragments are significantly internally excited SOCl radicals and chlorine atoms. The remaining fragments are generated *via* the $2\ ^1A'$ surface. Most fragments generated on this surface can be associated with a three-body decay producing chlorine atoms originating from $Cl_2(B\ ^3\Pi_{0+u})$ molecules which have been vibrationally excited above the dissociation limit, while the lesser portion produce $Cl_2(X\ ^1\Sigma_g^+)$ + SO($b\ ^1\Sigma^+$) and $Cl_2(B\ ^3\Pi_{0+u})$ + SO($X\ ^3\Sigma^-$) fragments. The spin-forbidden channel producing both ground state $Cl_2(X\ ^1\Sigma_g^+)$ + SO($X\ ^3\Sigma^-$) is not active.

Comparing the experimentally determined yields of the molecular, respectively the associated three-body decay channel and the radical channel to the calculated oscillator strengths of Table 2, the contribution of the former seems to be surprisingly small. However, in general, conclusions based on the calculated oscillator strengths remain necessarily speculative since the Franck–Condon factors for the excitation out of the vibronic ground state of $SOCl_2$ are unknown. With respect to the $2\ ^1A'$ state it must also be considered that it is not repulsive in the dissociation coordinate so that internal conversion or inter-system crossing might be important. Direct radiative deactivation into the $X\ ^1A'$ state is unlikely since no fluorescence of $SOCl_2$ has been reported in the literature.

(ii) Photolysis at 235 nm

Taking into account the accuracy of our calculations and the broadening of the vertical excitation energy range due to the short lifetime associated with repulsive states we conclude that for the excitation of $SOCl_2$ at 235 nm the $3\ ^1A'$, $4\ ^1A'$ and the $3\ ^1A''$ states should be accessible in addition to the states considered in the previous section.

From experimental evidence in REMPI imaging[14] and time-of-flight[16,45] studies it is clear that the radical channel is the dominant decay channel as it is the case for 248 nm dissociation. Cl and Cl* atoms were state-specifically detected with bimodal kinetic energy distributions. Basically, ground state Cl atoms are produced with low kinetic energy and a small positive β parameter of 0.2 ± 0.2,[16] while excited Cl* atoms are preferentially produced with large kinetic energy and a positive β parameter of 0.8 ± 0.2,[16] close to the limiting value for an instantaneous decay from the ground state geometry *via* an excited state of A″ symmetry. The fast fragments account for 30% (Cl) resp. 29% (Cl*) of the total yield of atomic chlorine.[16] The major portion of the remaining chlorine fragments appear as slow atoms with $\beta = 0.2$.[16] Fast ground state Cl atoms are believed to be produced by non-adiabatic long-range interactions from initially generated Cl* atoms due to their similar kinetic energy and spatial distributions.[14] In principle, such long range interactions can dramatically change the anisotropy parameter if only a fragment subset is concerned, as it was observed for the photodissociation of Cl_2O. For $SOCl_2$ however, the deviation of the anisotropy parameters for fast Cl and Cl* atoms is too small to justify the assumption of a similar mechanism to be operative. However, we believe that the previously proposed electronic state correlation model employed for the explanation of this observation based on Mulliken's treatment of HCl[46–48] is not applicable to $SOCl_2$ considering its reduced symmetry and the much larger number of accessible electronic states. In view of the large calculated oscillator strength of the $3\ ^1A''$ state it is likely that the dissociation at 235 nm proceeds *via* this higher lying state producing the same fragments as the $2\ ^1A''$ state. The kinetic energy content of the fast chlorine atoms necessarily correlates these products with a SOCl fragment carrying on average 50% of the available energy as internal excitation.[16] Since the fast chlorine atoms behave identically to the chlorine atoms produced in 248 nm photodissociation, it cannot be ruled out, however, that the fragmentation might proceed *via* the same excited $2\ ^1A''$ state.

Table 4 Speed distribution and the β anisotropy parameter of Cl and Cl* fragments for the 235 nm photodissociation of $SOCl_2$. T: trace in Fig. 5, v_0 and Δv: center and width of the Gaussian function used in the fit procedure described in the text

	Excited state	T	Dissociation channel	β (this work) abundance	β (ref. 16) abundance	v_0 /m s^{-1}	Δv /m s^{-1}
Cl	3 ^{1}A″	4	$SOCl_2 \rightarrow SOCl + Cl$	0.85 ± 0.08 28.3%		2540	650
	3 ^{1}A′	3	$SOCl_2 \rightarrow SOCl^* + Cl$	0.10 ± 0.13 17.2%	0.8 ± 0.2 30%	1810	690
	3 ^{1}A′	2	$SOCl_2 \rightarrow SOCl + Cl$	0.10 ± 0.12	0.2 ± 0.2 37%	1075	650
		1	$SOCl \rightarrow SO + Cl$	0.00 ± 0.07 19.5%		800	625
Cl*	3 ^{1}A″	4	$SOCl_2 \rightarrow SOCl + Cl^*$	0.68 ± 0.07 19.2%		2540	650
	3 ^{1}A′	3	$SOCl_2 \rightarrow SOCl^* + Cl^*$	0.10 ± 0.13 12.6%	0.8 ± 0.2 29%	1810	690
	3 ^{1}A′	2	$SOCl_2 \rightarrow SOCl + Cl^*$	0.10 ± 0.12	0.2 ± 0.2 4%	1075	650
		1	$SOCl \rightarrow SO + Cl^*$	0.00 ± 0.06 3.2%		800	625

Slow chlorine atoms are almost exclusively produced in the electronic ground state and are generated in a three-body decay correlating with $SO + Cl(^2P_{J'}) + Cl(^2P_{J''})$ as partner products. Since one three-body decay produces two chlorine fragments, and the total percentage of chlorine atoms produced in a three-body decay amounts to 41%, the contribution of the three-body decay to the overall fragmentation is 25%.[16] The value obtained in the present work is 22.7% and agrees very well with the previously determined value (*cf.* Table 4, traces 1 and 2). The excited state associated with the generation of slow chlorine atoms must be of A′ symmetry because the β parameter was found to be 0.2 ± 0.2.[16] Again, this behavior reminds of the behavior associated with 248 nm dissociation, nevertheless some significant differences cannot be ignored. First, $SO(X\ ^3\Sigma^-)$ fragments could only be observed in the vibrational levels $v = 0$ and $v = 1$.[16] This is in striking contradiction to the 248 nm case where vibrational levels up to $v = 7$ were found to be populated for lower excitation energy.[13] Thus, within the detection limit the vibrational state population of $SO(X\ ^3\Sigma^-)$ for 235 nm dissociation does not suggest the occurrence of a molecular decay at all. On the contrary, only SO was observable which can be associated with a three-body decay. Second, since SO was detected under collision-free conditions, the kinetic energy content of $SO(X\ ^3\Sigma^-)$ can be employed to calculate the energy content of the partner fragments. Again, the SO kinetic energy is so low that the partner fragments must be two separated chlorine atoms.[16] Therefore, we assume that the state which produces slow chlorine fragments in the 235 nm dissociation is the 3 ^{1}A′ state rather than the 2 ^{1}A′ state which is active at 248 nm.

In short, at 235 nm again two excited states of different symmetry and two decay channels are operative. The radical channel is likely to proceed *via* the 3 ^{1}A″ state. The participation of the 2 ^{1}A″ state which is accessed at 248 nm is unlikely. Fragments are excited Cl* atoms and internally excited SOCl radicals. Some Cl* is probably converted to ground state Cl in a non-adiabatic process at large internuclear distances. Slow ground state Cl atoms are produced in conjunction with $SO(X\ ^3\Sigma^-)$ *via* the 3 ^{1}A′ state. This is suggested by the absence of any evidence of a molecular decay. The associated two-body decay seems to be the radical channel instead. This will be further evidenced by the experimental results obtained in this work.

(iii) Photolysis at 193 nm

Previous experimental work has shown that in the photolysis at 193 nm all three dissociation channels (1) to (3) are active. The main channel is the three-body decay channel (3) which accounts for *ca.* 80% of all fragments which was determined in a PTS study.[12] The main portion is the decay into ground state $SO(X\ ^3\Sigma^-) + 2Cl(^2P_J)$ with the quantum yield of $SO(X\ ^3\Sigma^-)$ determined to be 0.73 ± 0.1.[13] These independently obtained values agree well with a third data set obtained from diode laser absorption where the branching ratio for $SO(a\ ^1\Delta)$ production and $SO(X\ ^3\Sigma^-)$ production was estimated to be 0.25.[22] Although production of $SO(b\ ^1\Sigma^-)$ has been reported in literature,[23] it will not be further discussed here due to its small abundance. It might be associated with the molecular channel accounting for less than 3% of all fragments in the PTS experiments.[12]

The remaining fragments are ascribed to the radical channel (2) with significant internal excitation.[12] Spatial fragment anisotropies were determined for $Cl(^2P_J)$ and SOCl and suggest an excited state of A″ symmetry being responsible for the radical and the three-body decay channels likewise.[12] It is very tempting to associate this state with the 5 ^{1}A″ state found to exhibit the largest oscillator strengths of all calculated excited states which would consequently be mainly responsible for the strong absorption feature C in Fig. 1. Nevertheless, due to the high excitation energy, in addition to the previously discussed states three more states are accessible which also might contribute to 193 nm dissociation to a lesser extent.

(iv) Competing channels in 235 nm photolysis

In the Results section it was already mentioned that the speed where the β parameter increases (*cf.* Fig. 3) from 0.1 to the maximum values of 0.85 (Cl) and 0.68 (Cl*) is higher than the speed dividing the fragment kinetic energy range (*cf.* Fig. 2) into the two- and the three-body decay regime. This difference deserves further attention because it will help to elucidate the role of the participating excited states.

Since the three-body decay cannot account for the intermediate fast $Cl(^2P_J)$ atoms above 1500 m s^{-1} with a β parameter of 0.1, this speed region must be further subdivided. First, as the simpler case, the two-body decay shall be discussed. According to the observed β parameter increase at about 2000 m s^{-1}, one Gaussian is fitted to the high speed region accounting for the two-body decay generating Cl and Cl* with high kinetic energy and a β value of 0.85 and 0.68, respectively. The mean centers of the Gaussians are at 2540 m s^{-1} with a mean width of 650 m s^{-1} (curves 4 in Fig. 5). The probability that Cl or Cl* will be released is $\phi(Cl^*) = 0.4$. The observed β parameter values of 0.68 and 0.85 are close to the theoretical limit of 0.7 for an instantaneous decay from the ground state geometry with a Cl–S–Cl bond angle of 97°. Hence the symmetry of the excited surface is of A″ symmetry and the transition dipole moment μ is perpendicular to the

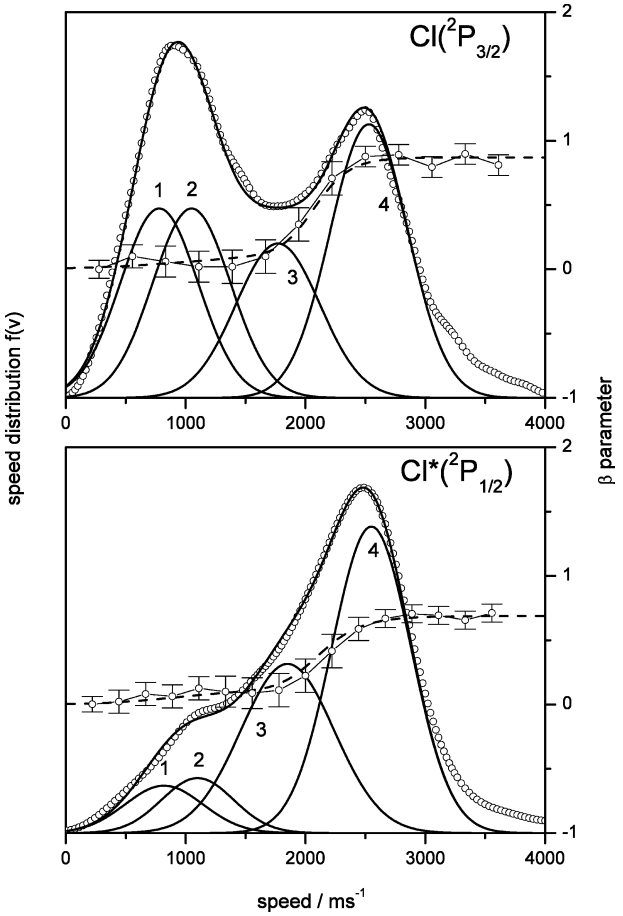

Fig. 5 Speed distributions and speed dependence of the β parameter (open circles) for ground state $Cl(^2P_{3/2})$ (upper panel) and excited state $Cl^*(^2P_{1/2})$ (lower panel) as shown in Fig. 2 and in Fig. 3. Solid lines are the result of a fit procedure employing the Gaussian functions listed in Table 4. Curves 4 describe the contribution of the radical channel proceeding *via* the $3\ ^1A''$ state. Curves 3 describe the radical decay associated with the three-body decay occurring on the $3\ ^1A'$ surface. Curves 2 and 1 describe fragments generated in the first, resp. in the second step of the asynchronously concerted three-body decay which also proceeds on the $3\ ^1A'$ surface. Widths, amplitudes and β parameters of the individual contributions are listed in Table 4.

plane of symmetry, oriented parallel to the line connecting the two chlorine atoms. The measured β value above the theoretical limit may hint at an excited surface with an increased Cl–S–Cl bond angle.

Generally, the low speed region below 2100 m s^{-1} may be divided into two parts by simple energetic considerations. Due to the dissociation energy, $Cl(^2P_J)$ atoms which are released *via* a three-body decay cannot receive speeds above 1500 m s^{-1}. Thus, atoms faster than 1500 m s^{-1} are released in a second two-body decay mechanism together with an internally excited SOCl*. This channel is characterized by a slightly positive β parameter of 0.1. According to this small β parameter, it is most likely that the intermediate fast $Cl(^2P_J)$ are released *via* the $3\ ^1A'$ state. The calculated β parameter for the transition from the ground state to the $3\ ^1A'$ state is 0.27, in good agreement with the slightly lower value observed in our experiment. Thus, one Gaussian is fitted to the intermediate speed range accounting for the second two-body decay. The Gaussians for Cl and Cl* are almost identical and a mean value of 1810 m s^{-1} for the center at a mean width of 690 m s^{-1} is obtained (curves 3 in Fig. 5).

Hence, two different two-body decay mechanisms are determined releasing firstly fast $Cl(^2P_J)$ plus internally cold SOCl and generating secondly $Cl(^2P_J)$ in conjunction with internally excited SOCl*. The ratio between the two different two-body mechanisms is *ca.* 1.5 : 1 for the first (curves 4) and the second (curves 3), respectively. The ratio is identical for Cl and Cl*.

In the three-body regime, fitting of the speed distributions depends on whether the decay is sequential or concerted.[17] If, for simplicity, we assume that the observed speed distributions can be described by a sum of Gaussian functions, then for a synchronously concerted decay with two equivalent $Cl(^2P_J)$ atoms a single Gaussian function should be sufficient to model the observed speed distribution in the three-body decay regime. However, attempts to fit the three-body contribution by a single Gaussian did not yield satisfactory results. If two Gaussians were fitted to the experimental data, with mean centers of the Gaussians at 800 and 1075 m s^{-1} and with mean widths of 625 and 650 m s^{-1} for slow and intermediate slow chlorine atoms, respectively (curves 2 and 1 in Fig. 5) the agreement with the experimental data was significantly better, suggesting a sequential or asynchronously concerted decay. In the three-body region the probability that Cl* will be released is rather small: $\phi(Cl^*) = 0.23$. The observed β parameter is about 0.1 for the chlorine atoms being generated in the first bond cleavage and close to zero for the chlorine atoms released in the second one, independently of their spin–orbit state. Detailed data are given in Table 4. The identical values for the β parameters for the slow two-body decay fragments (curves 3) and the fast three-body decay fragments (curves 2) suggest that these fragments are generated on the same $3\ ^1A'$ potential energy surface.

A more refined picture of the decay dynamics is now obtained. Instead of associating the three-body decay channel and the two-body decay channel with different excited states, we conclude that the $3\ ^1A'$ state predominantly produces three fragments *via* reaction (2) and two fragments *via* reaction (1) where the SOCl fragments are highly internally excited. The latter fragments are likely to carry predominantly vibrational and rotational energy and can be associated with those fragments previously suggested to be produced in a hitherto unobserved electronically excited state.[12] Fast $Cl(^2P_J)$ fragments in both spin–orbit states are probably generated on the $3\ ^1A''$ state *via* a fast and direct dissociation.

F. Conclusions

A comprehensive picture of the ultraviolet dissociation of the $SOCl_2$ molecule was obtained. Time-dependent density function theory calculations were employed to obtain the 10 lowest singlet electronic states along with their vertical excitation energies. New and existing experimental evidence has been interpreted by simultaneous excitation of electronic states. The picture of the $SOCl_2$ dissociation dynamics obtained from our treatment accounts for all existing experimental evidence. Also, the absorption spectrum can be rationalized by the most intense transitions.

Photodissociation at 248 nm simultaneously excites the $2\ ^1A'$ and the $2\ ^1A''$ states. The latter one is responsible for more than 80% of the fragments generating $Cl(^2P_J)$ atoms and internally excited SOCl radicals. The former accounts for the remaining fragments and mainly produces ground state SO(X) molecules in a three-body decay in conjunction with two chlorine atoms. A small portion also leads to electronically excited SO(b) or Cl_2(B) molecules in a molecular channel that can be regarded as a two-body decay associated to the main three-body decay. No evidence exists for the spin-forbidden joint production of two ground state SO(X) and Cl $_2$(X) molecules.

At 235 nm, the $3\ ^1A'$ and the $3\ ^1A''$ states are accessed. Approximately 25% of the parent molecules decay *via* the $3\ ^1A'$ state mainly into the three fragments $SO(X) + 2Cl(^2P_{3/2})$. A smaller portion produces $Cl(^2P_{3/2})$ in conjunction with highly excited SOCl. Here, the three-body decay associated two-body decay is the radical channel. Direct experimental evidence was found for this association from the speed dependence of the

anisotropy parameter derived from the 3D velocity vector distribution. The majority of the $SOCl_2$ molecules decays *via* the 3 $^1A''$ state to $Cl^*(^2P_{1/2})$ + SOCl. The SOCl radical carries significant internal energy while *ca.* 50% of the exited spin–orbit state $Cl^*(^2P_{1/2})$ atoms are converted to ground state $Cl(^2P_{3/2})$ by non-adiabatic long-range interactions.

At 193 nm, the three-body decay channel dominates the fragmentation process *via* excitation of the 5 $^1A''$ state. A minor fragmentation channel is the radical channel producing internally excited SOCl and a chlorine atom, probably *via* the same 5 $^1A''$ state. A small contribution of the molecular channel is also observed.

The detailed understanding of the $SOCl_2$ photodissociation dynamics could be achieved (1) because TDDFT calculations were performed allowing the prediction of excited state properties of $SOCl_2$ and (2) because sophisticated experiments were performed allowing to determine the full 3D velocity vector distribution. The combination of these tools is the key to understanding complex fragmentation schemes with several overlapping electronic states and several competing fragmentation channels.

Acknowledgements

The authors are grateful to Dr M. Roth for many stimulating discussions and to Dr U. Titt for assembling the 3D imaging machine. T. S. E. thanks the Fonds der Chemischen Industrie for a personal grant, A. C. thanks the Alexander von Humboldt Foundation for financial support. Funding by the Deutsche Forschungsgemeinschaft is gratefully acknowledged.

References

1 A. Chichinin, T. S. Einfeld, C. Maul and K.-H. Gericke, *Rev. Sci. Instrum.*, 2002, **5**, 1856.
2 A. Chichinin, T. S. Einfeld, K.-H. Gericke and C. Maul, in *Imaging in Molecular Dynamics: Technology and Applications*, ed. B. J. Whitaker, Cambridge University Press, Cambridge, 2003, pp. 138–164.
3 T. S. Einfeld, C. Maul, K.-H. Gericke and A. Chichinin, *J. Chem. Phys.*, 2002.
4 L. Schäfer, N. Gödecke, O. Ott, C. Maul, K.-H. Gericke, P. S. Shternin, E. V. Orlenko and O. S. Vasyutinskii, *Chem. Phys.*, 2004, **301**, 213.
5 C. Maul, T. Haas, K.-H. Gericke and F. J. Comes, *J. Chem. Phys.*, 1995, **102**, 3238.
6 C. Maul, T. Haas and K.-H. Gericke, *J. Phys. Chem. A*, 1997, **101**, 6619.
7 T. S. Einfeld, A. Chichinin, C. Maul and K.-H. Gericke, *J. Chem. Phys.*, 2002, **116**, 2803.
8 T. Yamabe, S. Nagata, Y. Kikuzono and K. Fukui, *Bull. Chem. Soc. Jpn.*, 1975, **48**, 1349.
9 M. Kawasaki, K. Kasatani, H. Sato, H. Shinohara, N. Nishi, H. Ohtoshi and I. Tanaka, *Chem. Phys.*, 1984, **91**, 285.
10 R. J. Donovan, D. Husain and P. T. Jackson, *Trans. Faraday Soc.*, 1969, **65**, 2930.
11 X. Chen, F. Asmar, H. Wang and B. R. Weiner, *J. Phys. Chem.*, 1991, **95**, 6415.
12 G. Baum, C. S. Effenhauser, P. Felder and J. R. Huber, *J. Phys. Chem.*, 1992, **96**, 756.
13 H. Wang, X. Chen and B. R. Weiner, *J. Phys. Chem.*, 1993, **397**, 12260.
14 M. Kawasaki, K. Suto, Y. Sato, Y. Matsumi and R. Bersohn, *J. Phys. Chem.*, 1996, **100**, 19853.
15 A. P. Uthmann, P. J. Demlein, T. D. Aliston, M. C. Withiam, M. J. McClements and G. A. Takacs, *J. Phys. Chem.*, 197, **882**, 2252.
16 M. Roth, C. Maul and K.-H. Gericke, *Phys. Chem. Chem. Phys.*, 2002, **4**, 2932.
17 C. Maul and K.-H. Gericke, *Int. Rev. Phys. Chem.*, 1997, **16**, 1.
18 M. W. Chase, NIST-JANAF, Thermochemical Tables, 4th edn., *J. Phys. Chem. Ref. Data*, 1998, Monograph 9, Part I + II.
19 K. P. Huber and G. Herzberg, *Constants of Diatomic Molecules, Molecular Spectra and Molecular Structure IV*, Van Nostrand Reinhold, New York, 1979.
20 M. W. Wilson, M. Rothschild, D. F. Muller and C. K. Rhodes, *J. Chem. Phys.*, 1982, **77**, 1837.
21 Y. Endo, H. Kanamori and E. Hirota, *Chem. Phys. Lett.*, 1987, **141**, 129.
22 H. Kanamori, E. Tiemann and E. Hirota, *J. Chem. Phys.*, 1988, **89**, 621.
23 M. Bogey, S. Civis, B. Delcroix, C. Demuynck, A. F. Krupnov, J. Quiguer, M. Yu. Tretyakov and A. Walters, *J. Mol. Spectrosc.*, 1997, **182**, 85.
24 E. U. K. Gross, J. F. Dobson and M. Petersilka, *Density Functional Theory II*, Springer Series in Topics in Current Chemistry, ed. R. F. Nalewajski, Springer, Heidelberg, 1996.
25 A. D. Becke, *J. Chem. Phys.*, 1993, **98**, 5648.
26 M. J. Frisch, G. W. Trucks, H. B. Schlegel, G. E. Scuseria, M. A. Robb, J. R. Cheeseman, V. G. Zakrzewski, J. A. Montgomery, Jr., R. E. Stratmann, J. C. Burant, S. Dapprich, J. M. Millam, A. D. Daniels, K. N. Kudin, M. C. Strain, O. Farkas, J. Tomasi, V. Barone, M. Cossi, R. Cammi, B. Mennucci, C. Pomelli, C. Adamo, S. Clifford, J. Ochterski, G. A. Petersson, P. Y. Ayala, Q. Cui, K. Morokuma, P. Salvador, J. J. Dannenberg, D. K. Malick, A. D. Rabuck, K. Raghavachari, J. B. Foresman, J. Cioslowski, J. V. Ortiz, A. G. Baboul, B. B. Stefanov, G. Lui, A. Liashenko, P. Piskorz, I. Komaromi, R. Gomperts, R. L. Martin, D. J. Fox, T. Keith, M. A. Al-Laham, C. Y. Peng, A. Nanayakkara, M. Challacombe, P. M. W. Gill, B. Johnson, W. Chen, M. W. Wong, J. L. Andres, C. Gonzales, M. Head-Gordon, E. S. Replogle and J. A. Pople, *GAUSSIAN 98 (Revision A.11.1)*, Gaussian Inc., Pittsburgh, 2001.
27 K. J. Palmer, *J. Am. Chem. Soc.*, 1938, **60**, 2360.
28 I. Hargittai, *Magy. Kem. Foly.*, 1968, **74**, 596.
29 I. Hargittai, *Acta Chim. Hung.*, 1969, **60**, 231.
30 S. Suzuki, M. Yamaguchi, M. Onda, T. Sakaizumi, O. Ohashi and I. Yamaguchi, *J. Mol. Struct.*, 1981, **73**, 41.
31 F. Mata and N. Carballo, *J. Mol. Struct.*, 1983, **101**, 233.
32 M. B. Robin, *Higher Excited States of Polyatomic Molecules*, Academic Press, New York, 1974, **vol. I**, p. 293.
33 G. W. Mines, R. K. Thomas and H. Thompson, *Proc. R. Soc. London, Sect. A*, 1972, **329**, 275.
34 S. E. Sobottka and M. B. Williams, *IEEE Trans. Nucl. Sci.*, 1988, **35**, 348.
35 O. Jagutzki, V. Mergel, K. Ullmann-Pfleger, L. Spielberger, U. Meyer, R. Dörner and H. Schmidt-Böcking, in *Imaging spectroscopy IV*, ed. M. R. Descour and S. S. Shen, Proc. SPIE, 1998, **3438**, 322.
36 M. Lampton, O. Siegmund and R. Raffanti, *Rev. Sci. Instrum.*, 1987, **58**, 2298.
37 S. Arepalli, N. Presser, D. Robie and R. J. Gordon, *Chem. Phys. Lett.*, 1985, **118**, 88.
38 D. Ascenzi, P. M. Regan and A. J. Orr-Ewing, *Chem. Phys. Lett.*, 1999, **310**, 477.
39 P. M. Regan, S. R. Langfold, D. Ascenzi, P. A. Cook, A. J. Orr-Ewing and M. N. R. Ashfold, *Phys. Chem. Chem. Phys.*, 1999, **1**, 3247.
40 G. E. Busch and K. R. Wilson, *J. Chem. Phys.*, 1972, **56**, 3638.
41 C. Maul, *Phys. Chem. News*, in press.
42 R. Bersohn and S. H. Lin, *Adv. Chem. Phys.*, 1969, **16**, 67.
43 T. S. Einfeld, C. Maul, K.-H. Gericke and A. Chichinin, *J. Chem. Phys.*, 2002, **117**, 4214.
44 Z. Li, *J. Phys. Chem. A*, 1997, **101**, 9545.
45 M. Roth, *Untersuchung photoinduzierter Dreikörperzerfälle am Beispiel von Cl_2O und $SOCl_2$*, dissertation.de, Berlin, 2001 (http://www.dissertation.de/PDF/mr418.pdf).
46 R. S. Mulliken, *Phys. Rev.*, 1936, **50**, 1017.
47 R. S. Mulliken, *Phys. Rev.*, 1937, **51**, 310.
48 R. S. Mulliken, *J. Chem. Phys.*, 1950, **8**, 382.